Supplementary information

The Impact of Twisting on the Intersystem Crossing in Acenes: An Experimental and Computational Study

Partha Malakar[a], Veniamin Borin [a], Anjan Bedi [a,c], Igor Shapiro* [b], Ori Gidron* [a], and Sanford Ruhman* [a]

[a]*Institute of Chemistry, The Hebrew University of Jerusalem, Jerusalem, Israel.*

[b]*Fritz Haber Center for Molecular Dynamics, Institute of Chemistry, The Hebrew University of Jerusalem, Jerusalem, Israel.*

[c]*Current address: Department of Chemistry, SRM Institute of Science and Technology, Kattankulathur, Tamil Nadu, India.*

Table of Contents

Sample preparation 2
Transient absorption setup. 2
Computational methods 3
Absorption and pump spectra 5
TA spectra and kinetics 6
Integrated difference spectra 7
Anisotropy and exponential fitting 8
Displacement vector of the normal mode 12
CAM-B3LYP calculated excited state absorption (from S1 minimum) spectra 14
Electron density difference 14
Second derivative of the absorption and TA spectra 15
The time cut near 600 nm and its mono exponential fitting 15

Sample preparation

the materials are synthesized according to the procedure reported by Bedi et al.[1] Sample solutions in acetonitrile were deaerated by purging with nitrogen for 20 min. The optical density of the sample at the excitation wavelength of 400 nm was kept around 0.2 to 0.3. The Transient absorption experiments were conducted in a 0.5 mm path-length rotating cell equipped with 1 mm quartz windows. The optical cell has been rotated rapidly during measurement in order to limit the photodecomposition. The absorption and emission spectra are provided in Figure S1.

Transient absorption setup.

TA measurements were carried out on a 1 kHz repetition rate home-made multipass amplified Ti-Saphire laser system. The fundamental was centred at 800 nm having pulse duration of 30 fs and 1 mJ pulse energy. The fundamental output was split in two. One portion pumped an Optical Parametric Amplifiers (TOPAS, Light conversion) whose signal output was centered at 1250 nm. A small fraction of the OPA output was focused on a 2 mm CaF_2 flat to generate a supercontinuum probe extending from 350 nm to 1000 nm. The other half was frequency doubled in a 0.1 mm thick BBO crystal and separated from the fundamental by reflection from 3 dielectric high reflectors @ 400nm. Transmitted probe pulses were dispersed in an Acton SP2150i imaging spectrograph onto a linear back thinned CCD camera (Entwicklungsbuero Stresing). A chopper operating at 500 hz blocks half of the pump pulses, and difference absorption spectra (ΔOD) are obtained as $\Delta OD = \log\left(\frac{I_{NP}}{I_P}\right)$ at each pump – probe delay which is computer controlled by a precision optical delay. P and NP designate probe intensity in presence and absence of a pump pulse respectively.

A 1/2λ wave plate on the fundamental arm prior to frequency doubling controlled the relative polarization of pump and probe fields. TA data was collected both in vertical and perpendicular mutual pump-probe polarizations. From these the magic angle absorbance difference spectra and its anisotropy were calculated as follows:

$$\Delta OD_{MA} = \frac{\Delta OD_{VV} + 2\Delta OD_{VH}}{3} \quad ; \quad r = \frac{\Delta OD_{VV} - \Delta OD_{VH}}{\Delta OD_{VV} + 2\Delta OD_{VH}}$$

At early time delays periodic modulations in the data were observed over a broad spectral range. These were assigned to impulsively excited coherent vibrational wave packets, either in the ground or excited state. The vibrational modulations were extracted as follows. A slowly varying background was obtained by fitting time traces at each probe wavelength to a fourth order polynomial, and then subtracted from the experimental data. This was performed from a delay of 350 fs and onwards to avoid interference from the coherent artefact surrounding pump-probe temporal overlap. The oscillating residual was Fourier transformed using an FFT algorithm in LabView 2012 after the residual was zero padded to the data length times 16.

Computational methods

The geometries of the full size compounds were optimized using the range-separated functional CAM-B3LYP[2] on the ground state (S_0), first excited (S_1) and lowest triplet (T_1) states with a def2-SVP basis set as implemented in the Gaussian16 program package[3]. Vertical excitation energies and oscillator strengths from S_0 and S_1 states were calculated with Gaussian16, while similar information concerning transitions from S_1-S_n was obtained using the Q-Chem 5.2[4] program. Simulated absorption spectra were obtained by convolution with a 0.15 eV FWHM Gaussian line-shape. Changes in the molecular structure upon $S_0 \rightarrow S_1$ excitation were resolved in terms of Huang-Rhys factors (HRF) S_j, dimensionless parameters defined as:

$$S_j = \frac{d_j^2}{2}$$

where d_j is a dimensionless displacement of the j^{th} normal mode. Bigger HRF corresponds to a larger geometrical change along a certain normal mode. This analysis was performed using MOMAP version 2020A software.[5,6,7,8,910]

A smaller model that was reduced to an anthracene was used for the excited state relaxed scan due to high computational demand. To this end, the energies are at the ADC(2)/cc-pVDZ//CAM-B3LYP/def2-SVP level of theory. The *ab initio* polarization propagator of the second order in its resolution-of-the-identity formulation (RI-ADC(2))[11] method was used from Turbomole 7.3 program.[12] For selected points of the relaxed scan the spin-orbit coupling matrix element between S_1 and T_2 states for the parent anthracene system (20 and 40 degrees twist) were calculated using ORCA 4.2[13] program by NEVPT2[14] method. The underlying CASSCF wave function has an active space of 12 electrons in 12 orbitals. The wave function was state averaged for four singlet (S_0, S_1, S_2, and S_3) and four triplet states (T_1, T_2, T_3, and T_4).

Absorption and pump spectra

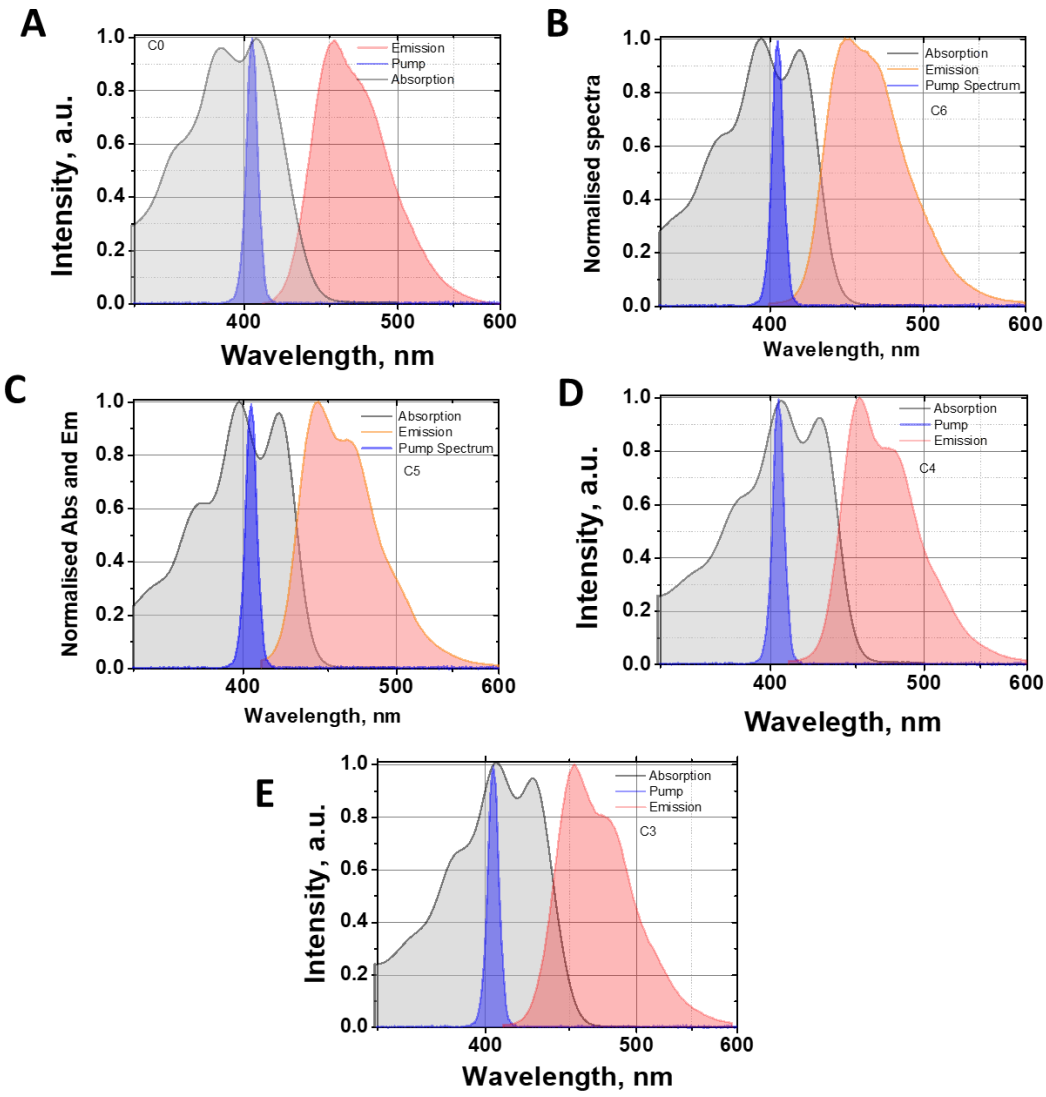

Figure S1: The absorption, emission and pump spectra of **Ant-C0**(A), **Ant-C6** (B), **Ant-C5** (C), **Ant-C4** (D), **Ant-C3** (E)

TA spectra and kinetics

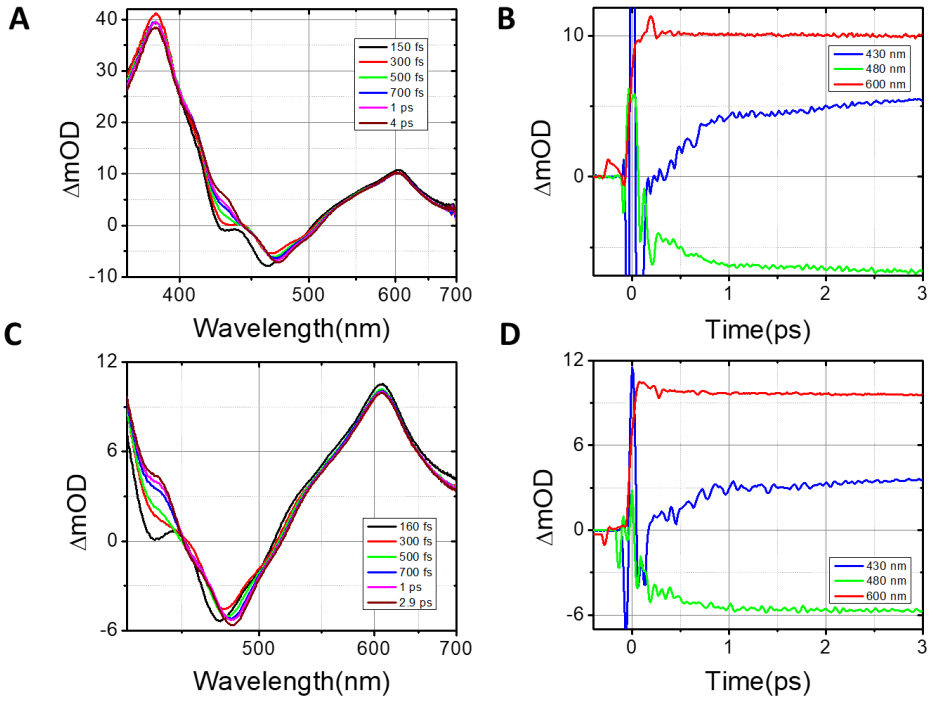

Figure S2: The transient absorption spectra (A) and time cuts (B) for **Ant-C5** in acetonitrile with magic-angle pump and probe polarizations. Same for **Ant-C4** in panels (C) and (D).

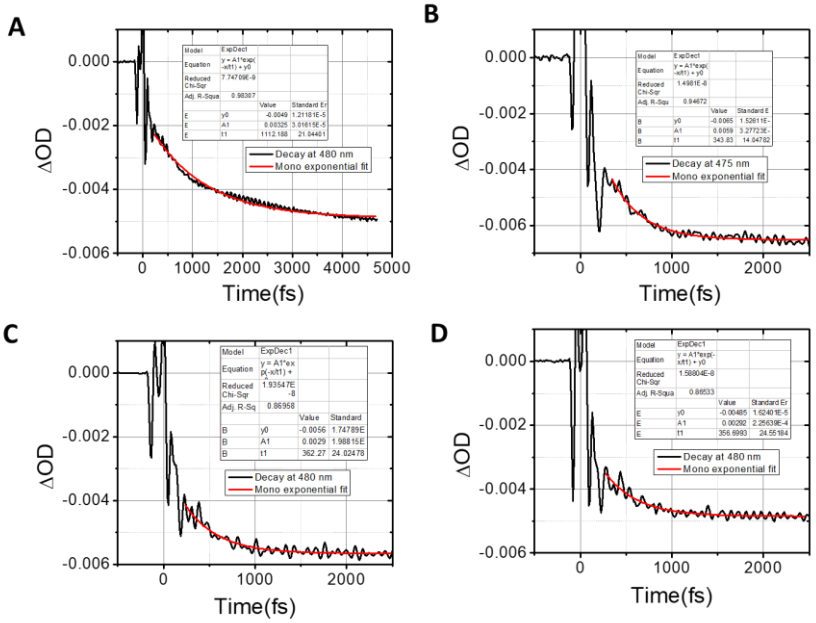

Figure S3: The time cut of TA data near emission maximum and the mono exponential fit of **Ant-C0** (A), **Ant-C5** (B), **Ant-C4** (C), **Ant-C3** (D).

Integrated difference spectra

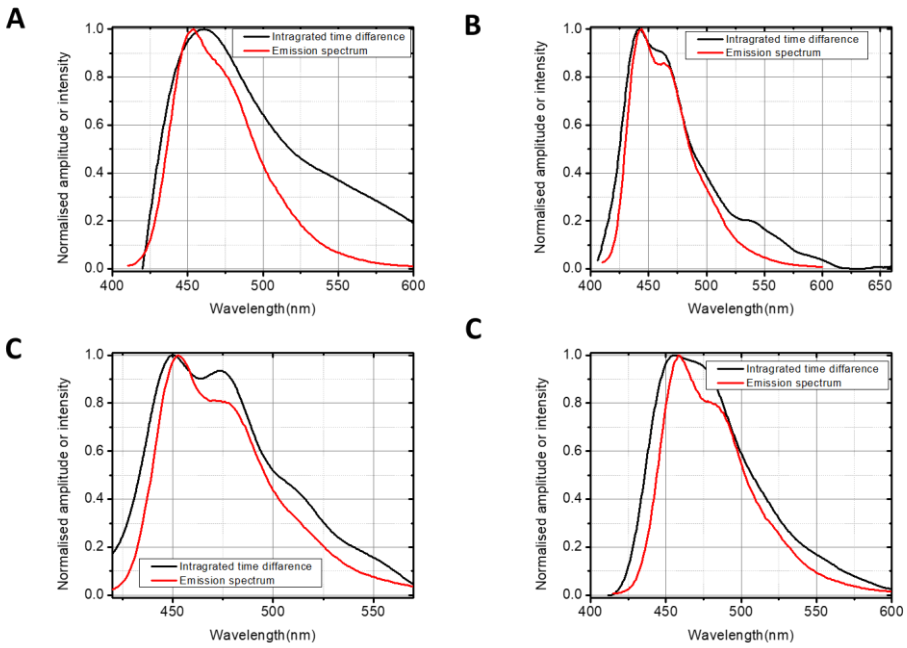

Figure S4: integrated time difference between 3ps and 400 fs for **Ant-C0** (A), **Ant-C5** (B), **Ant-C4** (C), **Ant-C3** (D). The magic angle spectra was for the analysis.

Anisotropy and exponential fitting

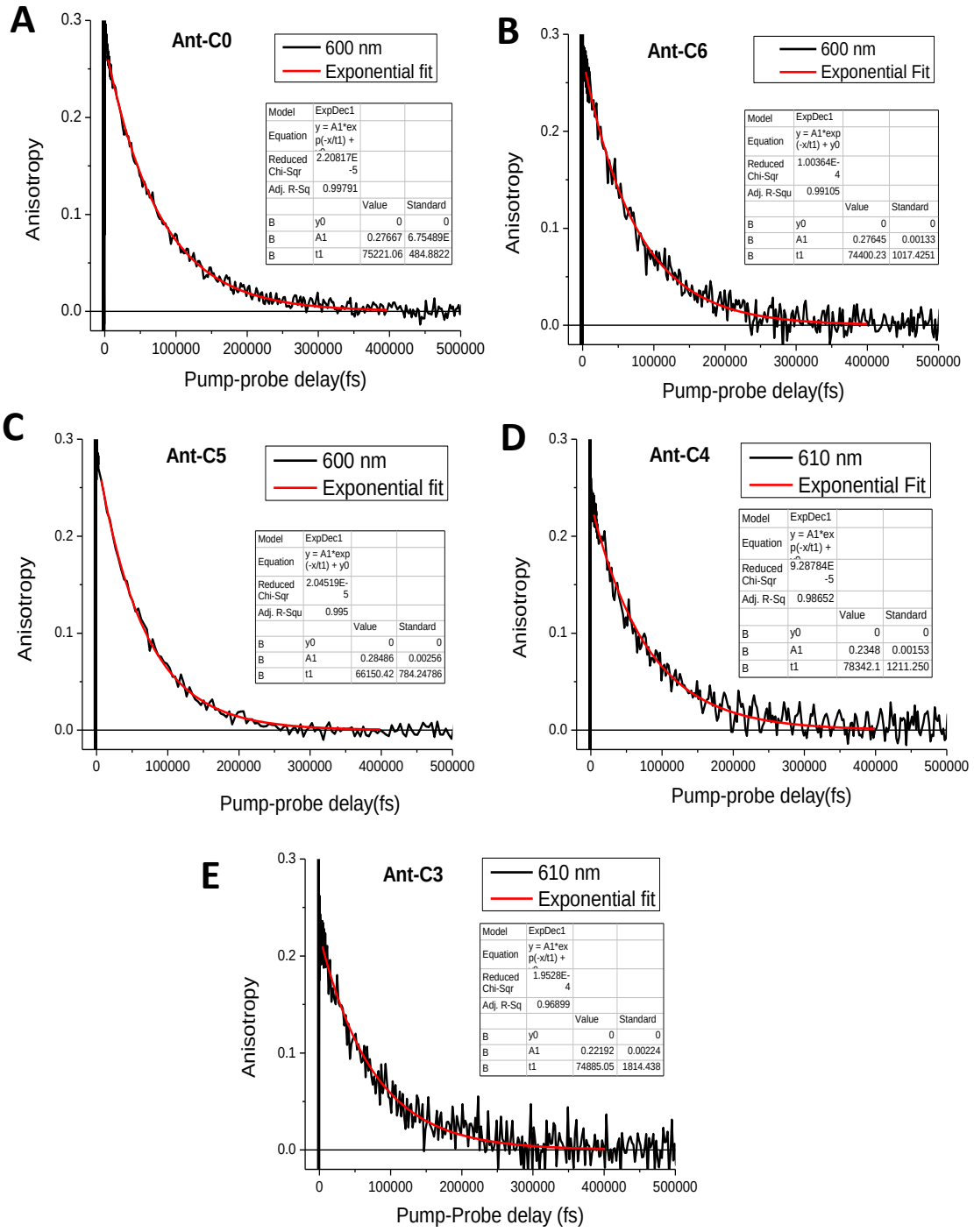

Figure S5: Anisotropy decay and its mono exponential fitting of **Ant-C0**(A), **Ant-C6** (B), **Ant-C5** (C), **Ant-C4** (D), **Ant-C3** (E).

Coherent vibrations.

coherent modulations were isolated from slowly varying background signals for each dispersed probe wavelength. After FFT the results were combined in a color coded 3 dimensional mapping where X- and Y-axes present wavelength in nm, and vibronic frequency in cm^{-1} respectively, and the Fourier power is color coded. Results obtained for **Ant-C4** are presented in Figure 3a. The vibrational coherence frequencies obtained can be assessed by integrating the spectra along the pump wavelengths ranging from 420-500 nm where the modulation activity is most intense. The resulting impulsive vibrational spectra are presented in Figure 3b for VV and VH pump-probe experiments. Both spectra exhibit bands at 140, 180, 214, 310, 395, 405, 420, 488 and 520 cm^{-1}, cutoff above by time resolution along with an intense solvent band at 379 cm^{-1}. Pure anthracene has Raman active vibrations at 242, 284, 391, 395, 477, and 519 cm^{-1}. Bands at 519, 395, and 391 are skeletal bends and CCC out of the plane deformations.[15] Despite similarity in frequencies, there is no one to one correlation with the measured modulations, nor are the exact mode frequencies for the twistacenes themselves known.

The map in Figure 3a helps to identify the electronic state upon which the vibrational wave packets are generated. Our experiment primarily probes transmission changes in a wavelength range dominated by absorption and emission from the excited state with only a marginal coverage of the red end of ground state absorption. The appearance of low frequency vibronic activity with structured pump wavelength dependence extending deep into the probe band is consistent with it stemming from coherent wave-packet motions on the excited state. Care is required in this assignment since extension of ground state Raman activity beyond the confines of ground state absorption due to population of excited S_0 vibrational levels is a common theme.[16] However given the low frequencies of the motions under study, such extensions will be limited in range. Further support for this view comes from the variation of FFT intensity

with probe wavelength. As shown in Figure S6, the modulations at 180, 214, and 310 all have a double peaked intensity pattern with a node in between at ~455 nm. These lobes appear to coincide with vibronic maxima in the fluorescence spectrum, strengthening assignment to wave packet motions on the directly photo-excited S_1.

To see how tethering impacts these displaced low-frequency modes these modulations must be compared on equal footing. This is complicated by solvent interference which varies widely due to changes in concentration of the different samples. We chose as a scaling marker the 310 cm-1 band appearing prominently in all spectra because of its obviously arising from the excited state of the solute, its intensity and spectral isolation making it immune to beating with nearby features, and its apparent insensitivity to changes in the tethering length. Accordingly all spectra were scaled to produce an equal intensity in this band. This was followed by the described procedure of Fourier analysis including integrating FFT power over a probe wavelength range from 420-480 nm. Results are shown for marker normalized spectra from all compounds in Figure 3c. One of the clearest changes is a systematic increase in the intensity of broad low frequency bands which appear to blue shift and gain intensity with tightening of the forced twisting.

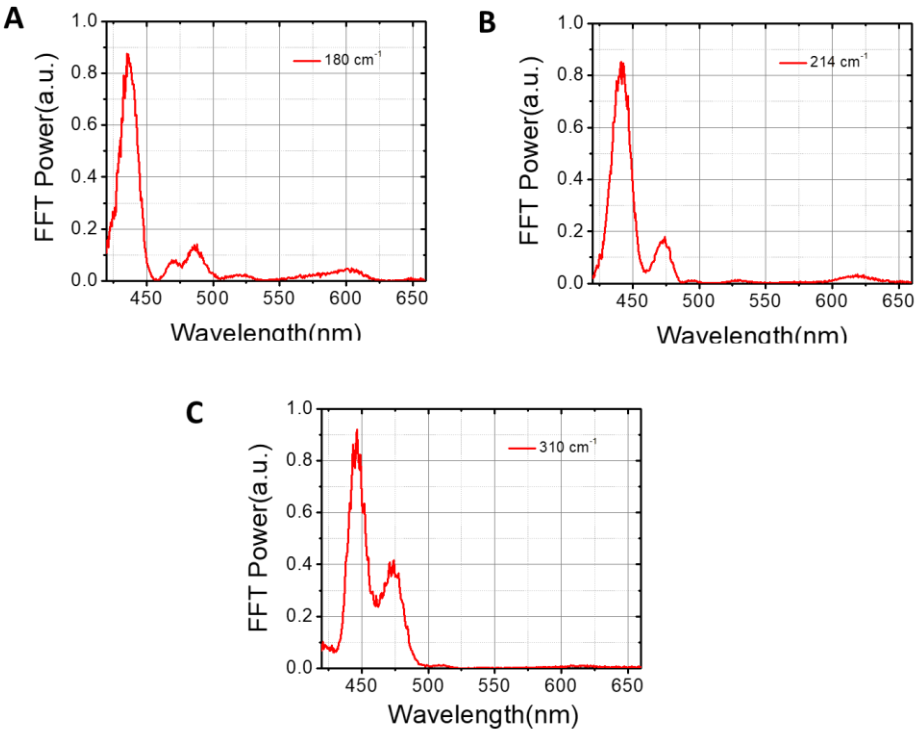

Figure S6: The spectra represent the variation of FFT power with the probe wavelength for **Ant-C4** for various vibrational frequency.

Displacement vector of the normal mode

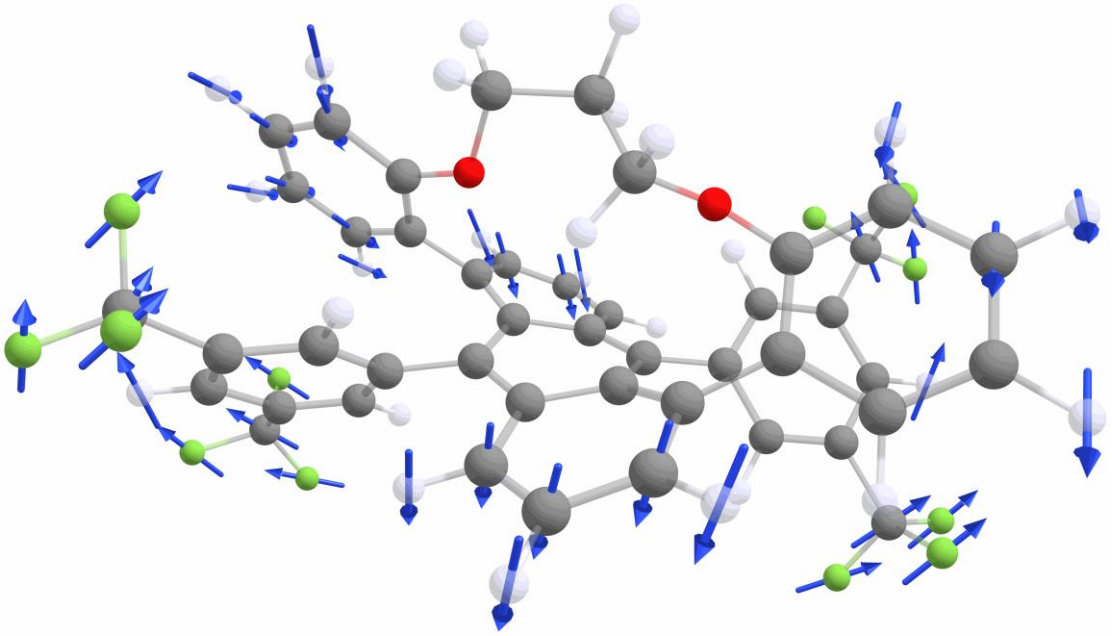

Figure S7. Displacement vector of the normal mode at 10 cm^{-1} (on the example of ***Ant-C3*** system).

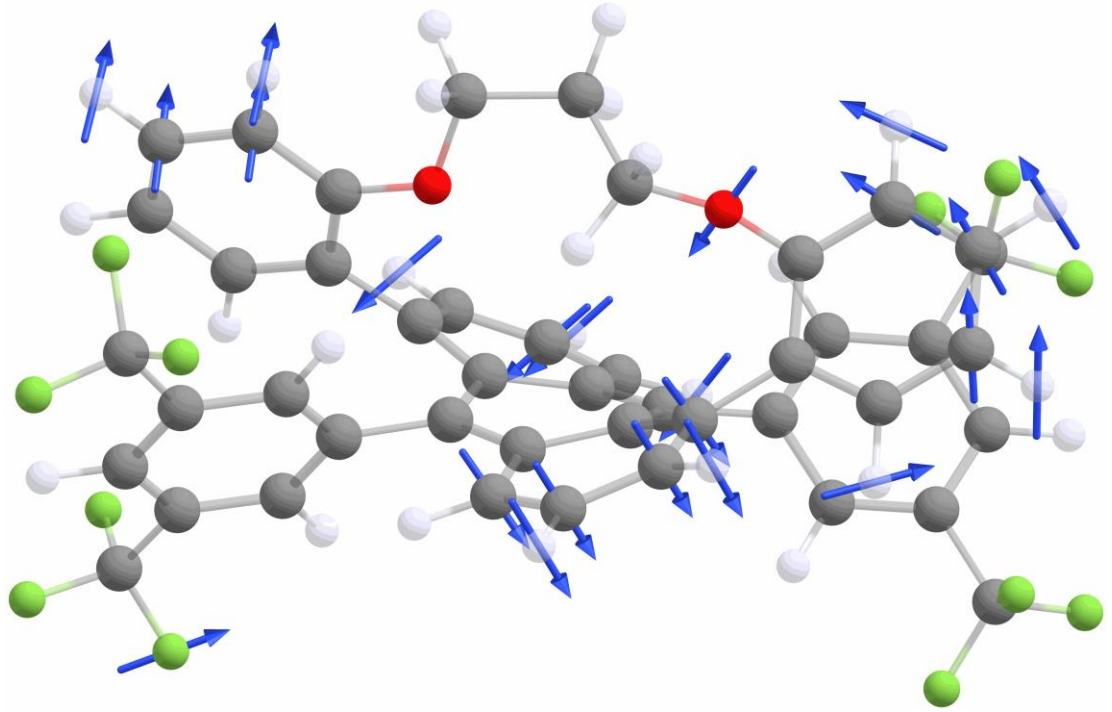

Figure S8. Displacement vector of the normal mode at 61 cm^{-1} (on the example of ***Ant-C3*** system).

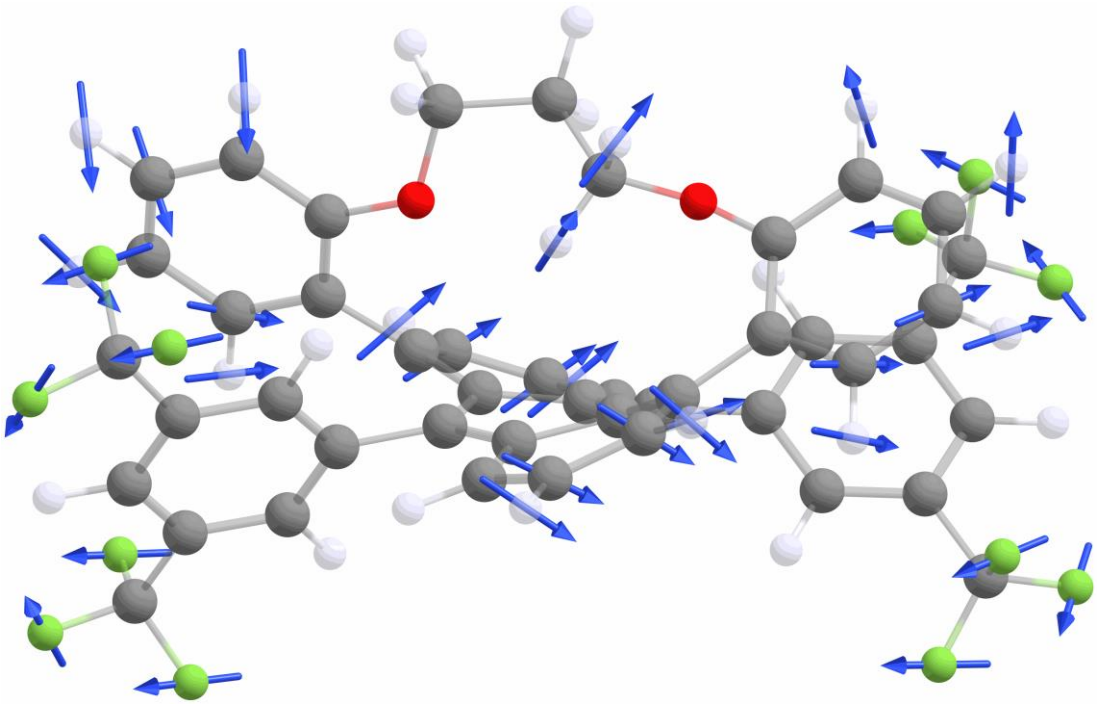

Figure S9. Displacement vector of the normal mode at 100 cm^{-1} (on the example of ***Ant-C3*** system).

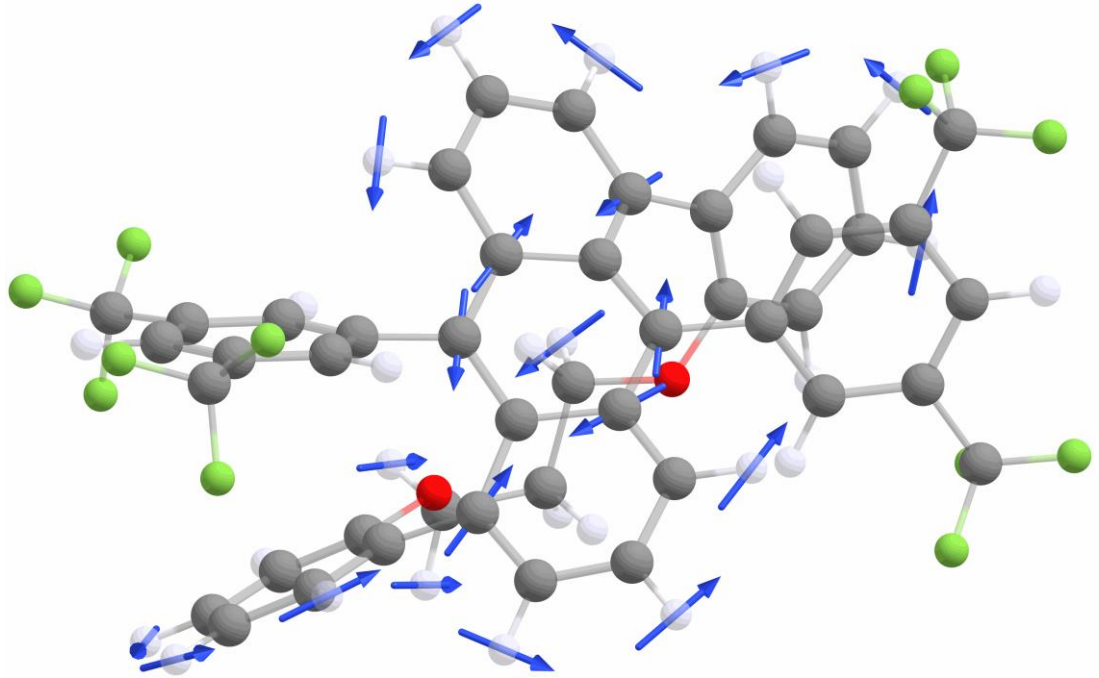

Figure S10. Displacement vector of the normal mode at 1410 cm-1 (on the example of ***Ant-C3*** system).

CAM-B3LYP calculated excited state absorption (from S1 minimum) spectra

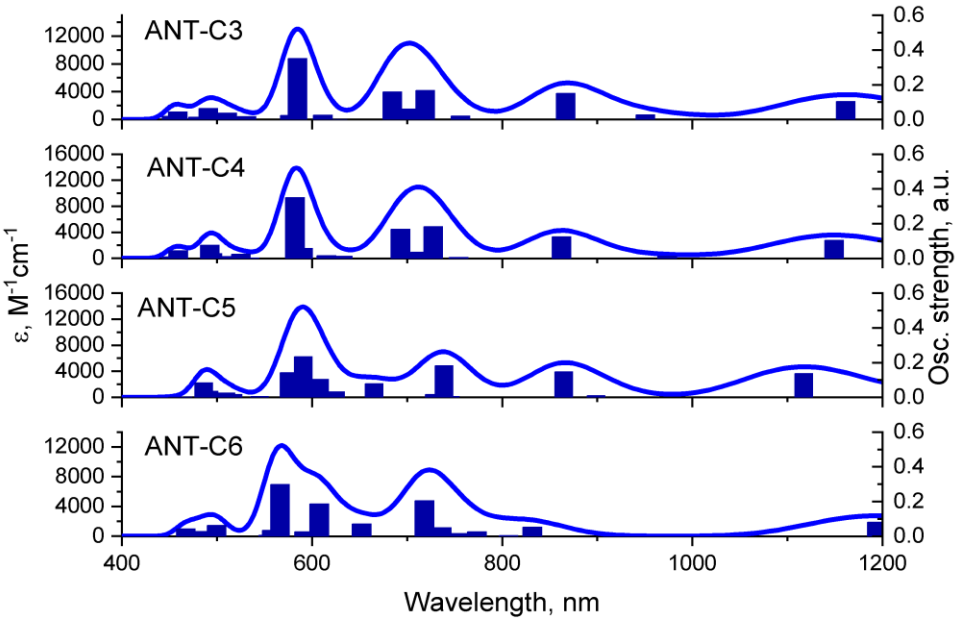

Figure S11. CAM-B3LYP calculated excited state absorption (from S1 minimum) spectra of **Ant-C3** (top) through **Ant-C6** (bottom) compounds. The sticks represent transitions to higher electronic states and their heights are scaled according to the oscillator strength.

Electron density difference

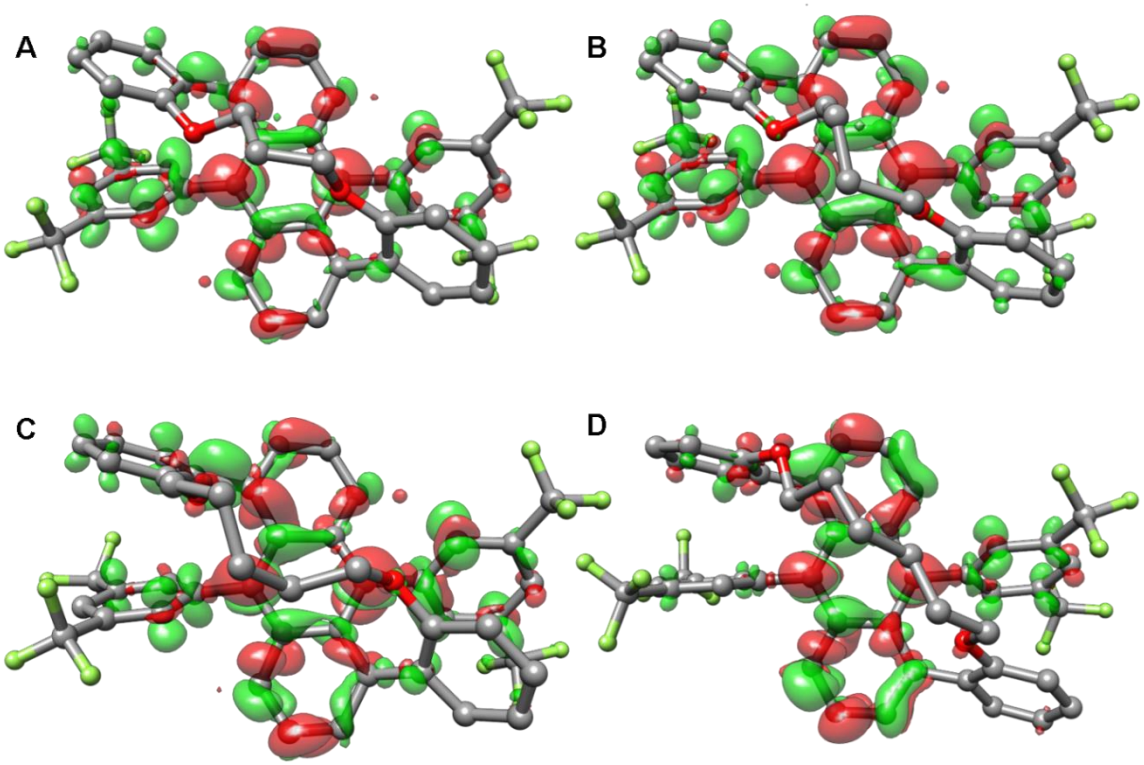

Figure S12. Electron density difference computed for A) S_{12}-S_1 in **Ant-C3** ; B) S_{13}-S_1 in **Ant-C4**; C) S_{12}-S_1 in **Ant-C5**; D) S_{14}-S_1 in **Ant-C6**. Green color represents a positive and red color a negative difference between the densities.

Second derivative of the absorption and TA spectra

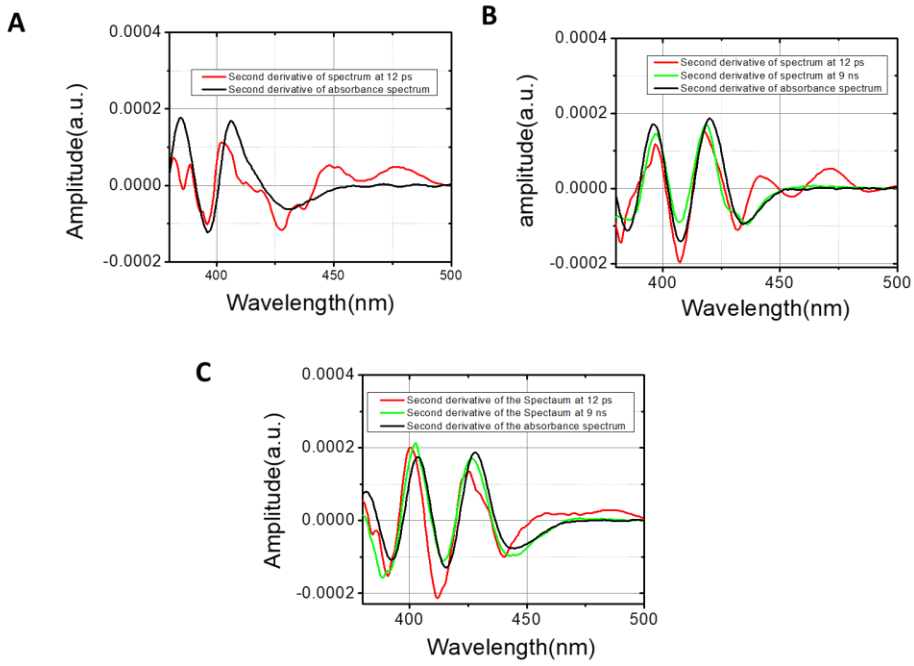

Figure S13: Second derivative of the spectra for **Ant-C0** (A), **Ant-C5** (B) and **Ant-C3** (C).

The time cut near 600 nm and its mono exponential fitting

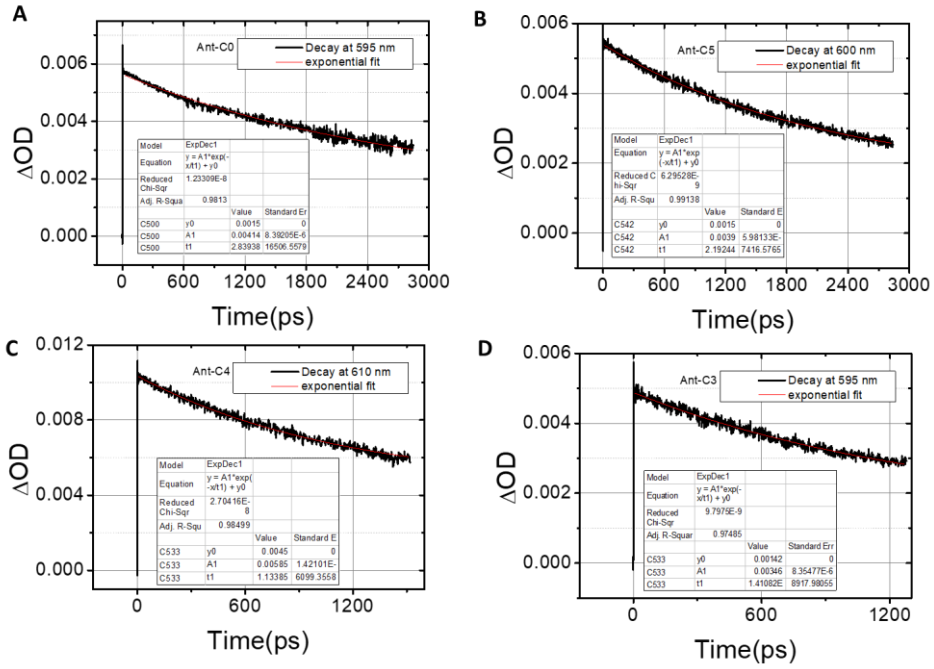

Figure S14: The time cut near 600 nm and its mono exponential fitting of **Ant-C0**(A), **Ant-C5** (B), **Ant-C4** (C), **Ant-C3** (D). The data were presented in magic angle polarisation.

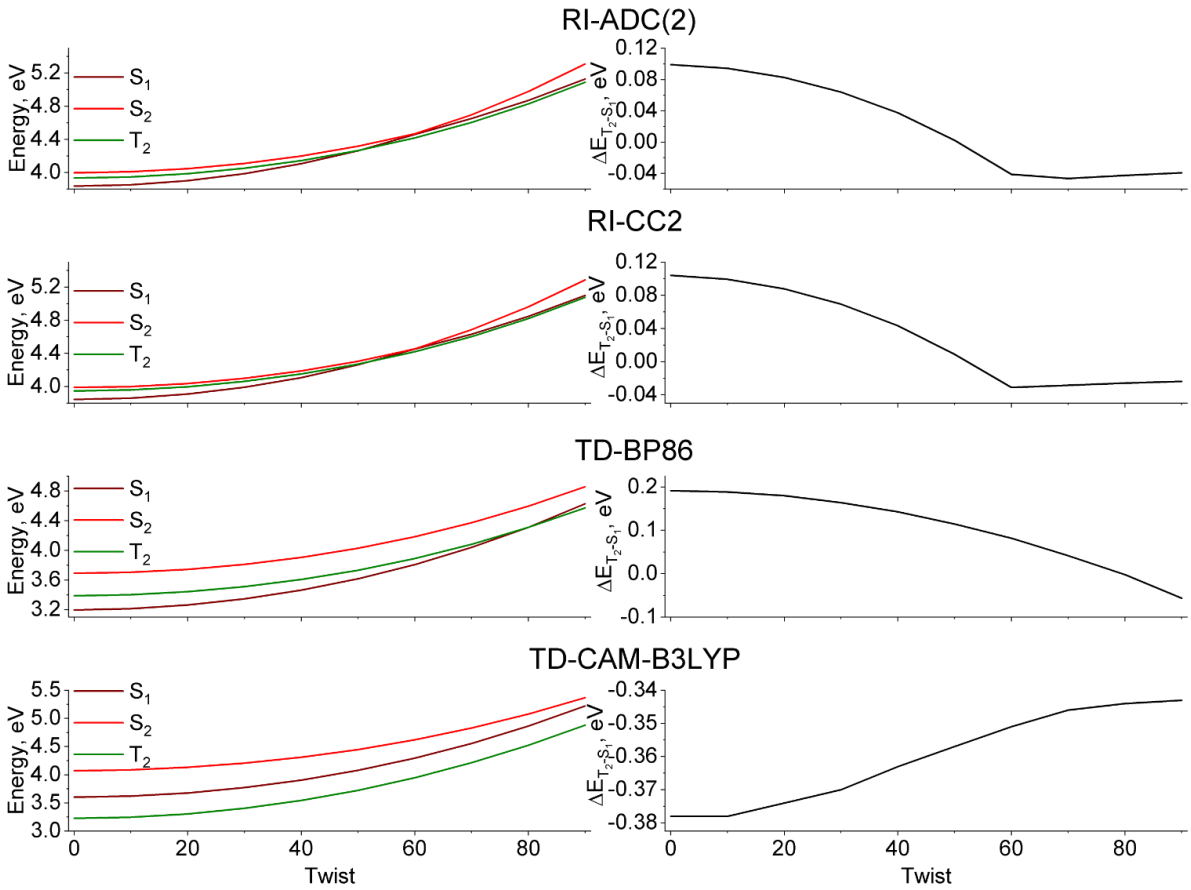

Figure S15: Relaxed scan of S_1, S_2, and T_2 (left) and the energy difference between T_2 and S_1 (right) computed at the CC2/cc-pVDZ, RI-ADC(2)/cc-pVDZ as well as TD-DFT with BP86/cc-pVDZ and CAM-B3LYP/cc-pVDZ levels of theory.

References

1 Bedi, A.; Shimon, L. J. W.; Gidron, O. Helically Locked Tethered Twistacenes. *J. Am. Chem. Soc.* **2018**, *140* (26), 8086–8090.

2 Yanai, T.; Tew, D.P.; Handy, N.C. A new hybrid exchange–correlation functional using the Coulomb-attenuating method (CAM-B3LYP). *Chem. Phys. Lett.* **2004**, *393*, 51-57.

3 Frisch, M. J.; Trucks, G. W.; Schlegel, H. B.; Scuseria, G. E.; Robb, M. A.; Cheeseman, J. R.; Scalmani, G.; Barone, V.; Mennucci, B; Peterssonet G. A. *et al.*, Gaussian 16 Revision A.03, Gaussian, Inc., Wallingford CT, 2016

4 Y. Shao, Z. Gan, E. Epifanovsky, A. T. B. Gilbert, M. Wormit, J. Kussmann, A. W. Lange, A. Behn, J. Deng, X. Feng, D. Ghosh, M. Goldey P. R. Horn, L. D. Jacobson, I. Kaliman, R. Z. Khaliullin, T. Kús, A. Landau, J. Liu, E. I. Proynov, Y. M. Rhee, R. M. Richard, M. A. Rohrdanz, R. P. Steele, E. J. Sundstrom, H. L. Woodcock III, P. M. Zimmerman, D. Zuev, B. Albrecht, E. Alguire, B. Austin, G. J. O. Beran, Y. A. Bernard, E. Berquist, K. Brandhorst, K. B. Bravaya, S. T. Brown, D. Casanova, C.-M. Chang, Y. Chen, S. H.

Chien, K. D. Closser, D. L. Crittenden, M. Diedenhofen, R. A. DiStasio Jr., H. Dop, A. D. Dutoi, R. G. Edgar, S. Fatehi, L. Fusti-Molnar, A. Ghysels, A. Golubeva-Zadorozhnaya, J. Gomes, M. W. D. Hanson-Heine, P. H. P. Harbach, A. W. Hauser, E. G. Hohenstein, Z. C. Holden, T.-C. Jagau, H. Ji, B. Kaduk, K. Khistyaev, J. Kim, J. Kim, R. A. King, P. Klunzinger, D. Kosenkov, T. Kowalczyk, C. M. Krauter, K. U. Lao, A. Laurent, K. V. Lawler, S. V. Levchenko, C. Y. Lin, F. Liu, E. Livshits, R. C. Lochan, A. Luenser, P. Manohar, S. F. Manzer, S.-P. Mao, N. Mardirossian, A. V. Marenich, S. A. Maurer, N. J. Mayhall, C. M. Oana, R. Olivares-Amaya, D. P. O'Neill, J. A. Parkhill, T. M. Perrine, R. Peverati, P. A. Pieniazek, A. Prociuk, D. R. Rehn, E. Rosta, N. J. Russ, N. Sergueev, S. M. Sharada, S. Sharmaa, D. W. Small, A. Sodt, T. Stein, D. Stück, Y.-C. Su, A. J. W. Thom, T. Tsuchimochi, L. Vogt, O. Vydrov, T. Wang, M. A. Watson, J. Wenzel, A. White, C. F. Williams, V. Vanovschi, S. Yeganeh, S. R. Yost, Z.-Q. You, I. Y. Zhang, X. Zhang, Y. Zhou, B. R. Brooks, G. K. L. Chan, D. M. Chipman, C. J. Cramer, W. A. Goddard III, M. S. Gordon, W. J. Hehre, A. Klamt, H. F. Schaefer III, M. W. Schmidt, C. D. Sherrill, D. G. Truhlar, A. Warshel, X. Xua, A. Aspuru-Guzik, R. Baer, A. T. Bell, N. A. Besley, J.-D. Chai, A. Dreuw, B. D. Dunietz, T. R. Furlani, S. R. Gwaltney, C.-P. Hsu, Y. Jung, J. Kong, D. S. Lambrecht, W. Liang, C. Ochsenfeld, V. A. Rassolov, L. V. Slipchenko, J. E. Subotnik, T. Van Voorhis, J. M. Herbert, A. I. Krylov, P. M. W. Gill, and M. Head-Gordon. *Advances in molecular quantum chemistry contained in the Q-Chem 4 program package. Mol. Phys*. **2015**, 113, 184–215

5 Niu, Y.; Li, W.; Peng, Q.; Geng H.; Yi, Y.; Wang, L.; Nan, G.; Wang D.; Shuai Z., *Molecular Physics*, **2018**, doi: 10.1080/00268976.2017.1402966.

6 Peng, Q.; Yi, Y.; Shuai, Z.; Shao, J., *J. Am. Chem. Soc.*, **2007**, 129, 9333-9339.

7 Niu, Y.; Peng, Q.; Shuai, Z., *Sci. China, Ser. B*, **2008**, 51, 1153-1158

8 Shuai, Z., *Chin. J. Chem.*, **2020**, 38, 1223-1232.

9 Shuai Z.; Peng Q., *Phys. Rep.*, **2014**, 537, 123.

10 Shuai Z.; Peng Q., *Nat. Sci. Rev.*, **2017**, 4, 224

11 Schirmer, *J. Phys. Rev. A: At., Mol., Opt. Phys.*, **1982**, *26*, 2395 —2416.

12 TURBOMOLE V7.3 2018, a development of University of Karlsruhe and Forschungszentrum Karlsruhe GmbH, 1989–2007, TURBOMOLE GmbH, since 2007, available from http://www.turbomole.com.

13 ORCA – an ab initio, density functional and semiempirical program package, V. 4.0.0, F. Neese, MPI für Chemische Energiekonversion, Mülheim A. D. Ruhr, Germany, 2017.

14 Angeli, C.; Cimiraglia, R.; Evangelisti, S.; Leinenger, T.; Marlieu, J.-P. *J.Chem.Phys*, **2001**, *114*, 10252.

15 Räsänen, J.; Stenman, F.; Penttinen, E. Raman Scattering from Molecular Crystals—II. Anthracene. *Spectrochimica Acta Part A: Molecular Spectroscopy* **1973**, *29* (2), 395–403.

16 Pollard, W. T.; Dexheimer, S. L.; Wang, Q.; Peteanu, L. A.; Shank, C. V.; Mathies, R. A. Theory of Dynamic Absorption Spectroscopy of Nonstationary States. 4. Application to 12-Fs Resonant Impulsive Raman Spectroscopy of Bacteriorhodopsin. *J. Phys. Chem.* **1992**, *96* (15), 6147–6158.